Lithos 206–207 (2014) 52–64

Contents lists available at ScienceDirect

Lithos

journal homepage: www.elsevier.com/locate/lithos

Invited review article

Advances in Fourier transform infrared spectroscopy of natural glasses: From sample preparation to data analysis

F.W. von Aulock [a,b,*], B.M. Kennedy [a], C.I. Schipper [f], J.M. Castro [e], D. E. Martin [g], C. Oze [a], J.M. Watkins [d], P.J. Wallace [d], L. Puskar [g], F. Bégué [a], A.R.L. Nichols [c], H. Tuffen [h]

[a] Department of Geological Sciences, University of Canterbury, PB 4800, Christchurch 8140, New Zealand
[b] School of Environmental Sciences, University of Liverpool, Liverpool, UK
[c] Research and Development Center for Ocean Drilling Science, Japan Agency for Marine Earth Science and Technology (JAMSTEC), 2-15 Natsushima-cho, Yokosuka, Kanagawa 237-0061, Japan
[d] Department of Geological Sciences, University of Oregon, Eugene, OR 97403, USA
[e] Institute of Geosciences, Johannes Gutenberg University Mainz, J.-J.-Becher-Weg 21, D-55128 Mainz, Germany
[f] School of Geography, Environment and Earth Sciences, Victoria University of Wellington, Wellington 6012, New Zealand
[g] Australian Synchrotron, 800 Blackburn Rd, Clayton, VIC 3168, Australia
[h] Lancaster Environment Centre, Lancaster LA1 4YQ, UK

ARTICLE INFO

Article history:
Received 10 April 2014
Accepted 19 July 2014
Available online 30 July 2014

Keywords:
FTIR
Fourier transform infrared spectroscopy
Volcanic glass
Analytical methods
Volatiles

ABSTRACT

Fourier transform infrared spectroscopy (FTIR) is an analytical technique utilized to measure the concentrations of H and C species in volcanic glasses. Water and CO_2 are the most abundant volatile species in volcanic systems. Water is present in magmas in higher concentrations than CO_2 and is also more soluble at lower pressures, and, therefore it is the dominant volatile forming bubbles during volcanic eruptions. Dissolved water affects both phase equilibria and melt physical properties such as density and viscosity, therefore, water is important for understanding magmatic processes. Additionally, quantitative measurements of different volatile species using FTIR can be achieved at high spatial resolution. Recent developments in analytical equipment such as synchrotron light sources and the development of focal plane array (FPA) detectors allow higher resolution measurements and the acquisition of concentration maps. These new capabilities are being used to characterize spatial gradients (or lack thereof) around bubbles and other textural features, which in turn lead to new insights into the behavior of volcanic feeder systems. Here, practical insights about sample preparation and analysis of the distribution and speciation of volatiles in volcanic glasses using FTIR spectroscopy are discussed. New advances in the field of FTIR analysis produce reliable data at high spatial resolution that can be used to produce datasets on the distribution, dissolution and diffusion of volatiles in volcanic materials.

Contents

* Corresponding author.
E-mail addresses: F.von-aulock@liverpool.ac.uk (F.W. von Aulock), ben.kennedy@canterbury.ac.nz (B.M. Kennedy).

http://dx.doi.org/10.1016/j.lithos.2014.07.017
0024-4937/

1. Introduction

Volatiles are the driving force behind volcanic eruptions (Sparks, 1978). Dissolved volatiles drastically change the physical and chemical properties of silicate melts and magmatic rocks (Hess and Dingwell, 1996). Therefore, high spatial and quantitative resolutions are essential for understanding volcanic and magmatic processes from melting of the mantle wedge to the growth of bubbles in volcanic eruptions (e.g. Cashman and Sparks, 2013; Lowenstern, 1995; Plank et al., 2013; Wallace, 2005). Specifically, the spatial distribution of volatiles in volcanic glasses records diffusion processes and can provide a quantitative estimate of the timescales and temperatures of hydration or dehydration mechanisms; such as the growth of bubbles (Castro et al., 2005; Kennedy et al., 2010; McIntosh et al., 2014; Watkins et al., 2012), lifetime of diffusion pathways in high-temperature melts (Berlo et al., 2013; Cabrera et al., 2010; Castro et al., 2012), hydration of archeological artifacts (Liritzis and Laskaris, 2011; Stevenson and Novak, 2011) and natural volcanic glasses (von Aulock et al., 2013), or the formation of crystals (Castro et al., 2008; Gardner et al., 2012; Seaman, 2013; von Aulock et al., 2013; Watkins et al., 2008). Furthermore the analysis of volatiles dissolved in glassy melt inclusions is the main tool used to constrain the volatile contents of magmas and assist in the understanding of deeper magmatic processes (e.g. Wallace, 2005). For example, volatile contents of a population of glassy inclusions and groundmass record changes in volatile concentrations over time, temperature and pressure, and comparison between and among them can help to establish models of degassing during magma ascent (Gonnermann and Manga, 2005; Mormone et al., 2011; Newman et al., 1988; Rust et al., 2003).

Numerous studies discuss analytical tools that can be used to measure volatiles in volcanic rocks (e.g. Cherniak et al., 2010; Devine et al., 1995; Ihinger et al., 1994). Methods for analyzing H_2O and CO_2 include: Fourier transform infrared spectroscopy (FTIR; the focus of this review article) (Behrens et al., 1996; Nichols and Wysoczanski, 2007; Stolper, 1982a, 1982b), secondary ion mass spectrometry (SIMS) (Delaney and Karsten, 1981; Hauri et al., 2002; Hervig et al., 1989, 2003; Kilgour et al., 2013), Raman spectroscopy (Behrens et al., 2006), Karl Fischer titration (Turek et al., 1976; Westrich, 1987), thermo gravitational analysis (TGA) (Applegarth et al., 2013; Denton et al., 2009), and electron backscatter methods (Berlo et al., 2013; Humphreys et al., 2008; McIntosh et al., 2014). Apart from availability, funding and other personal considerations such as the experience of the user, there are specific strengths and drawbacks to each analytical method.

Fourier transform infrared (FTIR) spectroscopy measures the fundamental vibrations and associated overtones of the chemical species present in a sample in the infrared region of the electromagnetic spectrum. FTIR instrumentation is comparatively simple (unless a synchrotron source is used) and can deliver accurate and precise measurements with high spatial and quantitative resolutions (e.g. Devine et al., 1995; Ihinger et al., 1994; Newman et al., 1986; Stolper, 1982a, 1982b; Zhang, 1999). Specifically, a spatial resolution down to 3 μm can be achieved (Della Ventura et al., 2014; Miller and Smith, 2005). Discriminating different bonds in hydrous compounds is one of the major strengths of FTIR analysis and allows the quantification of hydrous species to determine equilibration timescales (Zhang et al., 2000) and recognize effects of low temperature hydration (Dixon et al., 1995). Depending on the absorption bands investigated and the sample thickness, the detection limit can be as low as 10 ppm for hydroxyl groups, molecular water or total water (at 3570 cm^{-1}) and 25–50 ppm for C as carbonate and as low as about 2 ppm for molecular CO_2. These values are only rough estimates based on experience and depend largely on other properties of the sample such as thickness and optical properties as discussed later. A major drawback of this method is related to sample preparation, which, in most cases requires a doubly polished, thin, unsupported wafer. Sample preparation can be challenging for very small samples (such as melt inclusions), fragile samples such as pumices or perlites, and for samples that need to be polished to very thin wafers. The measured values are directly proportional to the thickness and water content of the sample and for very thin samples the quality of the thickness measurements is often the biggest limitation to the accuracy of quantitative measurements.

Secondary ion mass spectrometry (SIMS) uses an ion gun to emit secondary ions from the surface of the analyzed material, and the secondary ions are then collected by a mass analyzer. Samples only need to be polished on one side. Both the spatial resolution and detection range can be extremely high on the micrometer scale with detection limits down to parts per million (ppm) (Cherniak et al., 2010; Hauri et al., 2002; Hervig et al., 2003). Accurate quantitative measurements require careful calibrations (often done in reference to FTIR data) and the matrix effects of natural glasses can be complicated, requiring standards of similar chemical compositions. A limitation of this method is that the characterization of water speciation is not possible (Hervig et al., 2003; Ihinger et al., 1994), but the SIMS method is capable of analyzing the hydrogen and carbon isotope ratios (e.g. Shaw et al., 2008).

Raman spectroscopy is based on molecular vibrations caused by the scattering of light from a sample (Ihinger et al., 1994). The use of a coherent light source (i.e., a laser) allows for higher spatial resolution than conventional FTIR, and calibrations for quantitative measurements are rapidly improving (e.g. Behrens et al., 2006; Di Muro et al., 2006; Le Losq et al., 2012). Before Raman spectroscopic measurements can be used as a reliable quantitative method, combined studies with FTIR are necessary to provide a reliable calibration.

A way of determining bulk water concentrations without the use of spectroscopic methods is to force complete degassing by heating the samples to high temperatures in a furnace. The released gas can then be detected by quantitative methods with low detection limits via Karl

Fischer titration (e.g. Turek et al., 1976; Westrich, 1987) or by thermogravimetric methods, wherein weight loss during heating may be accompanied by exsolved gas analysis using mass spectrometry (e.g. Denton et al., 2009), or by vacuum manometry. These techniques have commonly been used in calibrating the FTIR method for analysis of volcanic glasses (Ihinger et al., 1994). The advantages of this method are that it is inexpensive as it does not require sophisticated instrumentation and sample preparation. Also, the degassing temperatures potentially contain information about volatile species degassing patterns (Applegarth et al., 2013; Tuffen et al., 2012). However, the processes of degassing at high temperatures are not yet fully understood, nor are the impacts of sample preparation. The discrimination of water or carbon dioxide from other volatiles such as halogens can be difficult. Further disadvantages of this method are that it also measures adsorbed volatiles and the contents of fluid inclusions and minerals, in addition to the volatiles dissolved in the glass, and the method is also sample destructive.

Backscattering of atoms at the surface in nuclear microprobes used in elastic recoil detection (ERD) or Rutherford backscattering (RBS) can produce accurate and precise measurements of hydrogen contents in volcanic glass. For example, the study of Bureau et al. (2009) gives a limit of $4 \times 16\,\mu m^2$ as a maximum spatial resolution and 94 ppm as a detection limit. Recent studies show promising results in the use of backscatter electron analysis for measuring water concentrations in volcanic glass (Humphreys et al., 2008; McIntosh et al., 2014), but matrix effects and the impact of the polishing quality are not fully understood, therefore analyses have to be treated as qualitative. A nuclear microprobe technique has been used to analyze C in glasses using the $^{12}C(d, p)\ ^{13}C$ nuclear reaction (Spilliaert et al., 2006; Varela and Metrich, 2000; Varela et al., 2000). The minimum detection limit for carbon varies from 40 to 15 ppm, and the uncertainty (1σ) using reference basaltic glasses containing 300 and 100 ppm of carbon is 10%.

Despite a number of analytical methods being suited for volatile analysis in volcanic glasses, funding and availability often limit the choice. FTIR spectroscopy is a widely available, well-documented method and is, therefore, preferred by many scientists. The list of methods, however, is constantly growing, which makes it important to review the choice of analytical method regularly based on recent developments in literature and technology. Detailed reviews of the analytical methods mentioned exist as overview chapters (e.g. Cherniak et al., 2010; Della Ventura et al., 2014; Ihinger et al., 1994). Comparatively, the increasing possibilities for volatile analysis and the increasing body of literature available on analytical FTIR techniques make this an ideal method for many applications when measuring volatile contents of volcanic glass. In the following sections, we provide an overview of recent techniques and developments in FTIR and share our practical experience in sample preparation, measurement and analysis of the resultant data.

2. Fourier transform infrared spectroscopy

2.1. Absorbance spectroscopy

Infrared spectroscopy is based on the absorption of light due to characteristic vibrations of molecular species in the infrared spectral region. The *Beer–Lambert Law* (also called *Bouguer–Beer–Lambert Law* or simply *Beer's Law*) states that the absorbance A (dimensionless), which is the common logarithm of the ratio of the intensity of transmitted light I (dimensionless) over incident light I_0, is proportional to molar concentration c ($mol \cdot l^{-1}$), path distance of the light through the sample l (cm), and a constant, ϵ ($L \cdot mol^{-1} \cdot cm^{-1}$), the molar absorptivity of the sample.

$$A = -\log_{10}\frac{I}{I_0} = \epsilon \cdot l \cdot c. \tag{1}$$

Absorbance therefore is dimensionless, l is in cm, ϵ is in $L \cdot mol^{-1} \cdot cm^{-1}$, and concentration expressed as the molar concentration ($mol \cdot l^{-1}$). In Earth sciences, mass fractions (w in $kg \cdot kg^{-1}$) are more practical, which leads to:

$$w = \frac{A \cdot M}{\epsilon \cdot l \cdot \rho} \tag{2}$$

with M as the molar mass (in $g \cdot mol^{-1}$) of the absorber and ρ as the density (in $kg \cdot m^{-3}$). For quantitative measurements, the absorbance, density, thickness and the molar absorption coefficient of a sample are needed to determine the weight fraction of a substance such as water in a sample by infrared spectroscopy. In FTIR, all wavelengths of the spectral area are created by a Michelson interferometer and the produced interferogram is transformed into a spectrum by a Fourier transformation. In a Michelson interferometer, the incoming beam of light passes through a half translucent mirror (i.e. the beam splitter) and interferes with the incoming beam while the additional beam path oscillates. This creates an interference pattern of the wavelengths of interest within a short period of time. In contrast to a prism, the light does not have to pass through a small slit and the intensity of passing light remains high. Further, one interferogram contains absorbance data across the whole spectral region, and a set of tens of scans can be performed in seconds to minutes; the absorbance of all relevant species can therefore be measured at high signal-to-noise concurrently. For more specific information, Cherniak et al. (2010) and Ihinger et al. (1994) cover the basics of FTIR spectroscopy in more detail.

2.2. Absorbance

The characteristic vibrations of H and C species are usually elucidated by the absorption of light in the region of near- and mid-IR (at wavenumbers of 1400–8000 cm^{-1}). The vibrations of the volatile species can either be bending or stretching, or a combination of the two in two (e.g., OH^- and H_2O) or three dimensions (e.g. CO_3^{2-}), resulting in several peaks in an absorbance spectrum (see Fig. 2 and e.g. Nakamoto, 2006). In addition, vibrations show overtones at higher wavenumbers in the near-IR region (see Fig. 2). These overtone peaks are usually weaker (at constant volatile concentrations and thickness) and, in glasses, typically less convoluted than the absorption peaks in the mid-IR region (making them the preferred bands for quantitative measurements of species at high volatile contents if the background in the near-IR are well fit). The absorbance of each peak is measured by measuring the maximum difference between the peak and a baseline, or the area between the peak and a baseline. Baseline choice depends on the type of baseline used in constraining the chosen epsilon value. The most widely used is a linear baseline between the minima on each side of the peak. It is the easiest to define and most reproducible between workers. However, in steep areas and on shoulders, such as around the CO_3^{2-} peaks, it can be difficult to apply. Alternatively, baselines have been defined with a flexicurve (Di Matteo et al., 2004; Zhang et al., 1997), curve equations (e.g. Dixon et al., 1995) and using degassed samples that are otherwise equivalent to those being analyzed (e.g. Dixon et al., 1988).

2.3. Density

Water has a significant influence on the density of glasses (Ochs and Lange, 1999) and for water contents different to the measured glass or standard material with literature values the final glass density has to be calculated by iteration. The density of natural glasses can be modeled using the equations given by Lange and Carmichael (1987); Lange (1997), a model for silicate melts at high temperatures, by extrapolating to room temperature. Partial molar volumes can also be used from Ochs and Lange (1999). Densities of silicate glasses are complex and a number of factors have to be considered (Ardia et al., 2014; Ochs and Lange, 1999; Richet et al., 2000). Measurements can be used to verify bulk densities and Archimedian methodologies such as in Richet et al. (2000) and Lange and Carmichael (1987) are very precise and accurate.

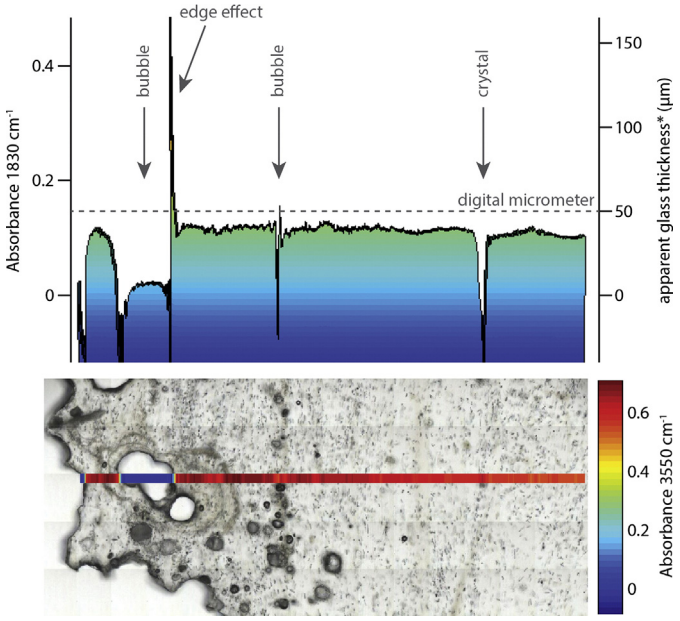

Fig. 1. Example of the use of absorbance on the 1830 cm^{-1} band for determining rhyolite glass thickness. Method, baseline fitting, and correlation between absorbance and thickness following Miwa and Toramaru (2013). Example is a rhyolite obsidian from the 2008 obsidian dome at Volcan Chaitén (Chile). Top panel shows apparent glass thickness as determined from the 1830 cm^{-1} that represents vibration of Si – O bonds. Bottom panel shows transmitted light photomicrograph of sample and absorbance on the 3550 cm^{-1} H_2O peak. Note that fluctuations in the determined thickness correspond to identifiable impurities and/or obstacles in the beam path (bubbles and crystals), so that the precision at each spectral measurement point is higher than with the digital micrometer (average thickness ≈ 50 μm). However, thickness measurements are subject to edge effects at component margins, and also to fluctuations in an automatically-fitted baseline (OPUS software package), so that some caution is required when interpreting the results.

A lot of standard laboratory scales can be modified for this purpose with readily available accessories that are user friendly.

2.4. Thickness

Thickness measurements are a major concern for thin samples as this can possibly introduce large errors in quantitative measurements (see Eqs. (1) and (2)). The most common methods for determining sample thickness are:

- Use of micrometers or digital displacement gauges: These are probably the most common ways to measure thickness, with a maximum accuracy of ± 2–3 μm. The main issue with these is that the pointed tip of the micrometer can break the sample if not used carefully. In addition, if the sample is very porous the tip can sink into the sample, both damaging it and making the measurement unreliable. By using a flat tip, this can be avoided, however, this will only measure maximum thickness in contact with the tip. It is also not confined to a small spot on the sample, and thus may not necessarily match to the position of the data collection. Nevertheless, for thick samples this is the most reliable and quickest method of gauging sample thickness and should also be performed as a reference measurement on all samples.
- Interference fringes: When using FTIR spectroscopy, counting the spectral fringes that are produced by interference of the primary source of light and the light of internal reflections within the sample allows the thickness to be accurately determined. Nichols and Wysoczanski (2007) determined a maximum standard derivation of ≈ 3 μm when compared with measurements with a digital displacement gauge. For a lot of samples, the internal reflections in the sample wafer are sufficient when measured in transmission mode, however, a higher signal-to-noise ratio of the interference fringes can be achieved when the sample is placed on a gold backing plate (to create a highly reflective surface for background measurements) and reflectance mode is used. The number of fringes can then be counted in a spectral region showing no chemical absorptions, for example with these samples the region between 2000 and 2700 cm^{-1} is commonly used, and the thickness determined using the following relationship:

$$d = \frac{m}{2n(\nu 1 - \nu 2)} \quad (3)$$

where m is the number of waves in a selected wavenumber range, n is the refractive index (dimensionless) of the sample and $\nu 1$ and $\nu 2$ (in cm^{-1}) are the highest and lowest wavenumbers respectively defining the selected interval (Wysoczanski and Tani, 2006). The largest contribution to error in these measurements is caused by the estimation of the refractive index (Nichols and Wysoczanski, 2007). This method can however be successfully used for glassy, well polished samples of

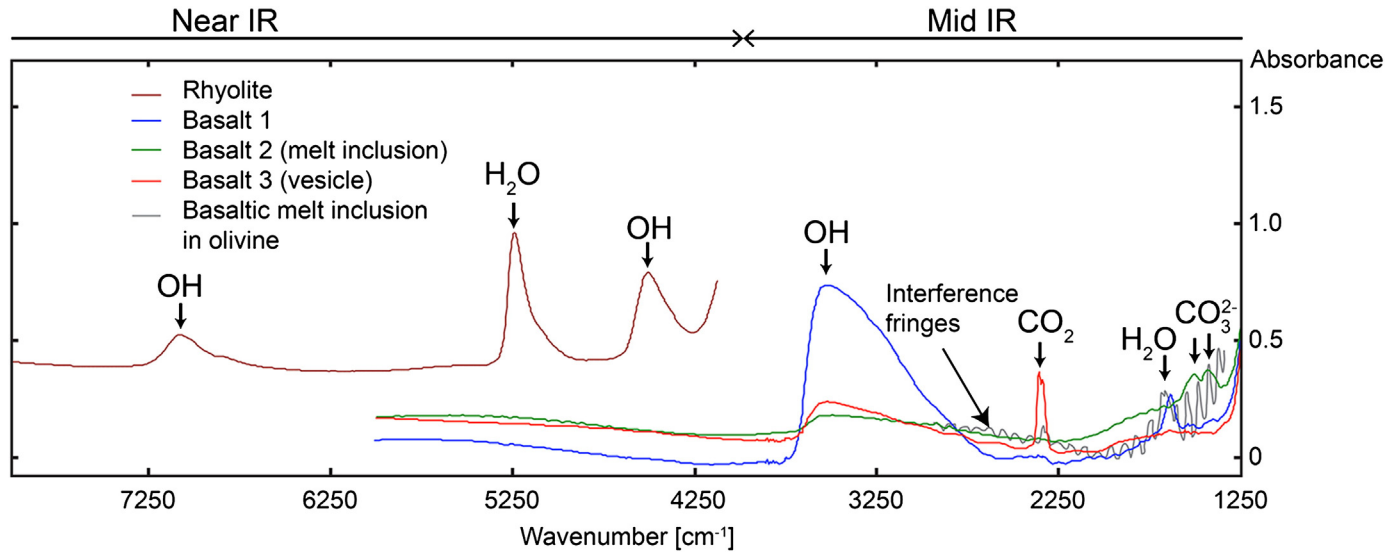

Fig. 2. Spectra of volcanic glass in the near- and mid-IR regions. The near-IR curve of a rhyolitic glass (brown) with total water contents of ≈ 4.3 wt.% shows the overtone and combination bands of hydroxyl and water. This is a thicker sample and therefore the absorbances are higher compared to the other curves. The mid-IR curves of basalt all show different contents in water and carbon dioxide species. The gray curve shows typical interference fringes in reflective mode.
This curve is adapted from Nichols and Wysoczanski (2007).

about 5–150 μm in thickness, where precision is higher for measurements of samples ≤100 μm (von Aulock et al., 2013). Commercial software such as OPUS by Bruker implements tools to automatically determine thicknesses based on interference fringes. This makes it a convenient method for the evaluation of large quantities of data in maps of samples with variable thickness. However, the peak count is highly dependent on the noise in the analyzed spectra and automatic data analysis might not provide sufficient control and transparency for scientific applications on natural samples.

- Calibrated microscope stages: z-calibrated stages of microscopes with visible-light capability can make very precise measurements of samples of almost any thickness, by measuring the vertical displacement between the focused surfaces of the wafer. Calibrations should be performed regularly to eliminate drift.
- Optical profilometers, which use interferometry and/or confocal microscopy to analyze surface topographies of small samples are commercially available, such as the Leica DCM 3D series and can have a vertical resolution of <4 nm (Ventura et al., 2012).
- Thickness determination using Si – O stretching on 1830 cm^{-1}: (Miwa and Toramaru, 2013) presented a calibration of thickness measurements that use the linear relationship between absorbance near the 1830 cm^{-1} band and the vibration of Si – O bonds in the glass (Zhang et al., 2002). By cross-correlation with thickness determined by reflectance interference fringes and digital micrometer, they determined the following relationship for thickness in an obsidian glass (Miwa and Toramaru, 2013):

$$d = 0.0340 \pm 0.0006 Abs_{1830}. \quad (4)$$

This technique has several limitations. It is not applicable to basalts, especially those that are hydrous, because the 1830 cm^{-1} is subordinate to, and partially overlapping with, the OH^- band at 1630 cm^{-1}, and has only been calibrated for one obsidian sample over a H_2O content range of 0.01 to 0.66 wt.% (Miwa and Toramaru, 2013). It does, however, have the potential to be very useful for automatic thickness determinations in high-SiO_2 glasses for several practical reasons. Firstly, the main strength of using reflectance to determine thickness is gained by having the reflectance interference fringes collected from the exact same analytical spot as the transmitted spectra; however, it may not always be possible to rapidly shift between transmitted and reflected modes on a given FTIR microscope. While quick changeover is possible on many desktop micro- and FPA-FTIR systems, the switchover is not straightforward on many synchrotron systems. Being able to use the 1830 cm^{-1} band on the transmitted light spectra thus circumvents the need to collect two types of FTIR spectra. For individual spot analyses, manual selection does not pose a major problem, but for FPA or map analyses, the number of spots makes manual correction of each spectrum impractical. Conversely, the measurement of peak absorption on a linear baseline — as is used in the 1830 cm^{-1} thickness determination allows automatic visualization of sample thickness variation just as one would automatically visualize volatile species distributions by selecting the appropriate peaks. In principle the volatile peaks in each spectrum within an FTIR image can be normalized to the 1830 cm^{-1} peak using the software, producing an image that represents concentration, assuming compositional homogeneity, and not just absorbance.

However, recent tests on a Chaitén (Southern Chile) low-vesicularity obsidian sample at the Australian Synchrotron that included traverses through obsidian glass and across bubbles and small clinopyroxene phenocrysts reveal potential issues (Fig. 1). Applying an automatic determination of sample thickness using the 1830 cm^{-1} peak with OPUS® software package does effectively yield a bulk thickness across clear portions of glass, but it does not clearly delineate the presence and size of the bubbles and/or clinopyroxene crystals (e.g. Fig. 1). Instead, the transmittance spectra deviate from linear baselines due to refraction about the non-orthogonal edges of the feature, causing artifacts in the thickness determinations, and the Si – O bonds in the clinopyroxene contribute to the absorbance on the 1830 cm^{-1} peak. These are important observations, because Miwa and Toramaru (2013) originally employed the 1830 cm^{-1} technique to determine effective glass thicknesses that eradicated the effects of microlites in the beam path, but the example shown in Fig. 1 suggests that this may not be an appropriate use of the otherwise valid technique. The use of the 1830 cm^{-1} vibrational signature of Si – O bonds holds a great deal of promise for automated thickness determination of high-SiO_2 glasses, but requires further development and careful applications to compositions different to those used for calibration by Miwa and Toramaru (2013).

- The thickness of melt inclusions can be measured by these techniques as long as they are exposed on both sides and there is no contamination from the host crystal in the FTIR spectra (Mormone et al., 2011). However, owing to their small size, it is often difficult to expose an inclusion on both sides. In order to ease sample preparation and dramatically increase the number of inclusions that can be targeted for FTIR analysis, several techniques have been developed to determine the thickness of partially exposed or unexposed inclusions.

Firstly, the thickness of melt inclusions can be measured by mounting the edge of a doubly polished wafer of the host crystal on to a needle using epoxy and immersing the wafer into a cylindrical glass well filled with refractive index liquid (Wallace et al., 1999). This allows the crystal to be rotated and viewed parallel to the flat dimension under a microscope with a calibrated eyepiece, thereby allowing a direct measurement of the thickness. These measurements have an accuracy of ≈1 to ≈3 μm, depending on how close a given inclusion is to the edge of the wafer. This method is time consuming, however, and very difficult to use with wafers that are thinner than ≈60 μm. If the above technique proves impractical due to the difficulty of handling small crystals, Befus et al. (2012) provide an alternative, which they term the X–Y proxy method. Inclusion thickness is approximated to the average of the horizontal (X–Y) dimensions of the inclusion. The major assumption of this method is that the inclusion has a regular polyhedral shape. This technique has been developed on inclusions hosted in quartz, but the principle should be applicable to inclusions in other host minerals, although checks are required.

The thickness of unexposed melt inclusions hosted in olivine can be measured indirectly using the technique of Nichols and Wysoczanski (2007). This involves firstly taking FTIR spectra through the unexposed, or partially exposed inclusion. The olivine present in the beam path will cause peaks on the spectra between 2000 and 1600 cm^{-1} due to Si – O overtone and combination bands. Then, without rotating the crystal, a second analysis is performed on the host olivine with no inclusion or groundmass glass in the beam path. The height of the peak at 2000 cm^{-1} within the Si – O overtone and combination bands is proportional to the amount of olivine in the beam path. By comparing the heights of this peak with and without the inclusion in the beam path, the proportion of the overall thickness made up by the inclusion can be calculated. Then, using the overall thickness of the crystal wafer at the points the spectra were taken, measured either directly, using a micrometer needle or a calibrated microscope stage, or indirectly, using interference fringes, the thickness of the inclusion can be calculated. The major drawback of this technique is that the Si – O overtone and combination bands of the olivine overlap with the molecular H_2O peak at1615 cm^{-1}. Thus if inclusion spectra are contaminated with olivine, molecular H_2O, and thus speciation, cannot be resolved. This method has been successfully applied to olivines (Nichols and Wysoczanski, 2007) and quartz (Befus et al., 2012). A similar technique is used by Agrinier and Jendrzejewski (2000) who rewrite the Beer–Lambert equation to incorporate the difference between the absorbance at 1710 cm^{-1} and the absorbance at 2234 cm^{-1} as a proxy for the sample thickness. They apply this technique successfully to basaltic glass but advise calibration of the method with a standard for other glass compositions.

2.5. Dealing with microcrystalline glasses

One issue with micro-FTIR is encountered when natural glasses contain small microlites of anhydrous phases. These can occur as discrete crystals in otherwise transparent amorphous glass, or as dense networks of tachylite glasses that nearly opaque, and are better described as networks of interlocking microcrystals with interstitial amorphous material, than pure glass. Traditionally, these common types of glasses are excluded from micro-FTIR analysis, although there have been several attempts to deal with this complexity. Semi-opaque glasses often have elevated baselines at high wavenumbers that can make spectra appear noisy, but that do not actually affect the heights of H_2O_t peaks in the mid-IR range, as diligently tested by Nichols et al. (2009) during differential scanning calorimetry experiments. This means that volatile abundances can be measured in such glasses as long as care is taken to correctly interpret the data: that is, to recognize that the H_2O contained in the bulk material is dissolved only in the residual glass portion of the material, not in the anhydrous microlites that make up a (potentially significant) proportion of the total sample thickness.

If the geological problem at hand requires only an estimate of the bulk volatile content of an opaque or microlite-bearing glass, micro-FTIR can be applied largely in the same way as for a hypocrystalline glass. Volatile distributions in these cases will represent bulk distributions resulting from the opposing and coupled processes of vesiculation and crystallization (e.g. Schipper et al., 2012). Alternatively, if the given geological application requires knowledge of the volatile contents in the residual domains of glass, the microlites must be removed from the total thickness of the sample to yield an effective thickness that is essentially the linear proportion of the thickness that is occupied by residual glass. Two methods for dealing with this issue have been applied. Miwa and Toramaru (2013) applied the 1830 cm^{-1} Si – O absorbance technique (see above) to microcrystalline vulcanian glasses under the assumption that absorbance would only be from glass in the beam path. The alternative approach has been to measure sample total thickness by a conventional method (usually micrometer), and then to subtract the proportion of microlites (± vesicles), as determined by backscatter electron SEM images on the regions of analysis (Hammer et al., 1999; Wright et al., 2007). These methods show promise, but require care in implementation and could benefit from rigorous testing.

2.6. Molar absorption coefficients

The molar absorption coefficient, ϵ, relates to the chemistry of the analyzed glass. Strictly speaking, ϵ should be determined for every sample. In most cases literature values for similar chemical compositions provide sufficient accuracy (see Table 1). If a new value ϵ has to be estimated, the volatile mass fraction in the glass needs to be measured by direct quantitative analytical methods such as Karl Fischer titration, RBS or H manometry. Any errors in the measurements of mass fraction, thickness or density will result in inaccuracies in ϵ and therefore be carried through all following measurements. Estimating absorption coefficients from equilibrated volatile species as reviewed by Cherniak et al. (2010) should only be used when volatile species ratios are well confined such as in some synthetic samples. Since the review article about volatile analysis in magma was released by Ihinger et al. (1994), a broader range of chemistries have been covered by reference measurements with a variety of analytical methods. Values for the ϵ exist for a range of compositions. Table 1 provides a summary of values for reference. The error for molar absorption coefficients varies depending on the way it was determined. Highest precision of the values in Table 1 are estimated for the values of the band at 3570 cm^{-1} at a median standard derivation of ± 2 l mol^{-1} cm^{-1}. Absorption coefficients of other bands show higher derivation in the listed studies of usually around 4–8 l mol^{-1} cm^{-1} and therefore, these literature values contribute most to the overall error of FTIR measurements on most volcanic glasses according to Agrinier and Jendrzejewski (2000). This also depends on the quality and thickness of the sample as well as on the methods used to determine the other parameters of the Beer–Lambert law.

3. Different modes of FTIR measurements

3.1. Transmission vs reflection FTIR spectroscopy

3.1.1. Transmission FTIR spectroscopy

Transmission FTIR spectroscopy is the most commonly used methodology for micro-FTIR applications in geological as well as in biological and chemistry applications. The data analysis is based entirely on the Beer–Lambert law (see Eq. (1)). As long as it is possible to prepare plane parallel, doubly polished thick section of appropriate thickness, transmission FTIR produces results that are less prone to instrumental variability, have a higher signal-to-noise ratio and can be used at higher spatial resolution. There is also a wider range of literature values for ϵ available.

3.1.2. Reflectance FTIR spectroscopy

To obtain the volatile content of samples that are difficult to polish on both sides (e.g. melt inclusions) with FTIR spectroscopy, samples can be studied using reflected light from the surface of a sample (Hervig et al., 2003; King and Larsen, 2013) or by using Attenuated Total Reflection (ATR) methods (Lowenstern and Pitcher, 2013). However, these methods only examine the surface of the sample and scattering effects can be difficult or impossible to correct for. In both reflection modes, the signal-to-noise ratio is smaller compared to transmission FTIR. This can be compensated by opening the aperture with the spatial resolution, and this makes the technique only applicable with larger melt inclusions or glassy samples. To account for instrumental variability in reflectance measurements, the peak at 3650 cm^{-1} can be normalized to the background at ≈4000 cm^{-1} (Hervig et al., 2003). To calculate the mass fraction of water in the sample, the calibration by Johnson et al. (2011) can then be used. The results in Johnson et al. (2011) show that data from reflectance measurements are overestimated by ≈0.4 wt.% H_2O (see Fig. 3) compared to transmission mode FTIR. The reflectance method has also proven useful for analysis of high pressure experimental charges (Weaver et al., 2011, 2013; Weber et al., 2011) or bubble evolution experiments (Mongrain et al., 2008).

3.2. Near-IR versus mid-IR

In most cases, the amount of water in the sample dictates which absorption band to use for analysis (see Fig. 5). Sample thicknesses have to be prepared accordingly to ensure high signal-to-noise ratios. As discussed earlier, high resolution imaging of water is not possible with low volatile concentrations, as this requires thick wafers where small textural features within the thickness of the sample can create apparent water heterogeneities (see Fig. 4).

Thin samples that could produce interference fringes within the spectra can also make analysis difficult. This is especially the case in the mid-IR region around 2500 ± 500 cm^{-1}, and makes the selection of an appropriate baseline for integration and quantification of the water in a sample difficult. If an aperture is used (i.e. in any method with conventional detectors), the diffraction limit of the measurements at low wavenumbers (≤2000 cm^{-1} Miller and Smith, 2005) limits the spatial resolution. If an FPA detector is used, higher spatial resolutions are not limited by the diffraction of long wavelengths (Miller and Smith, 2005). FPA detectors are mostly available for the mid-IR region, and similarly synchrotron sources are often set up for mid-IR measurements due to of a wider user base and the lower diffraction limit at the shorter wavelengths.

Table 1
Overview of available extinction coefficients (ϵ), modified and updated from Ihinger et al. (1994).

Volatile species	OH	H_2O	H_2O	OH	OH	H_2O	OH	H_2O	H_2O	CO_2	CO_3^{2-}	CO_3^{2-}	
Wavenumber [cm^{-1}]	7100	7100	5200	4500	4000	4000	3550	3550	1630	2350	1500–1700	1350–1430	
Newman et al. (1986)	0.32	0.184	1.61	1.73	1.14	1.07	100	56	55				Rhyolite
Integrated	96	83	248	341	290	350	44,000	26,300	2640				
Hauri et al. (2002)							90		56				Rhyolite
Okumura et al. (2003)							75						Rhyolite
Behrens et al. (2004)										1214			Rhyolite
Okumura (2005)				1.42	1.75								Rhyolite
Integrated				285	239								
Dobson et al. (1989)	0.26						88						Rhyolite
Ihinger et al., 1994			1.86	1.5			80						Rhyolite
Leschik et al. (2004)							80–136 C_{H_2Ot}						Rhyolite
Di Matteo et al. (2004)			1.36	1.58									Trachyte
Yamashita et al. (1997)			1.6	0.94			68						Dacite
King et al. (2002)			1.08	1.15			70.3		40.8		271	269	Andesite
Mandeville et al. (2002)			1.07	0.79			62.32		42.3				Fe-bearing andesite
Mandeville et al. (2002)			1.46	0.89			69.21		52.1				Fe-free andesite
Stolper (1982a, 1982b)	21	0.21	1.76	0.98	0.95	0.95	67	67					Basalt
Dixon et al. (1988)							63	63					Basalt
Dixon et al., 1995			0.62	0.67					25				Basalt
Jendrzejewski et al. (1996)							78						Basalt
Fine and Stolper (1985)											375	375	Basalt; Ca-Mg silicates
Cocheo (1994)			0.56	0.58									Basanite
Fine and Stolper (1985)										945	200	235	SiO_2–$NaAlSiO_2$
Integrated										25,200	24,100	16,800	glasses
Silver et al (1990)			1.87	1.43									Orthoclase
Silver and Stolper (1989)			1.67	1.13			70		49				Albite
Stolper et al. (1987)											199	235	Albite
Integrated											27,300	16,300	
Thibault and Holloway (1994)											355		Leucitite
Silver et al. (1990)			1.13	1.12									Jadeite
Fine and Stolper (1985)										945	200	235	SiO_2–Alb join

4. Sample preparation for transmission FTIR spectroscopy

4.1. Preparing your sample for optimal results

Sample preparation is the most time-consuming and important step in assuring successful measurements using FTIR transmission spectroscopy. A doubly polished wafer has to be prepared, where the two surfaces of the sample must be as parallel with each other as possible to reduce thickness variations. For glass samples, this is usually done by cutting the sample to create a flat surface or breaking it into small chips, polishing it on one side and then fixing it to a slide or other sample holder so the other side can be polished down to the final thickness. For melt inclusions, the procedure is the same, but involves using a single crystal or crystal fragment. The choice of thickness must be carefully considered and an appropriate adhesive for mounting the sample for polishing has also to be selected.

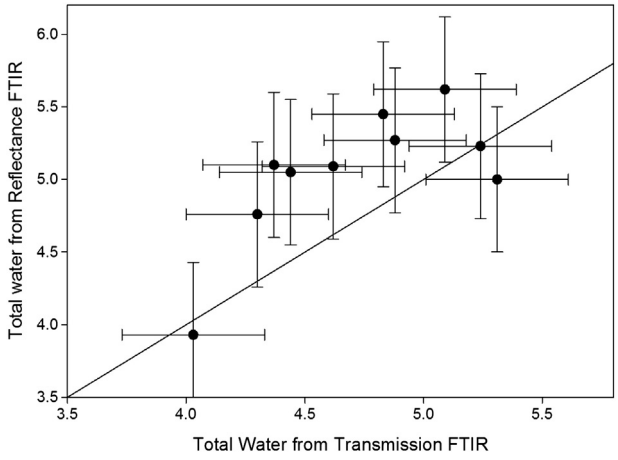

Fig. 3. Total water content in percent of melt inclusions measured with reflected and transmitted light in conventional FTIR at 3650 cm^{-1}. Errors are 0.5 wt.% and 0.3 wt.%. Figure modified from GSA data repository 2011107 of Johnson et al. (2011).

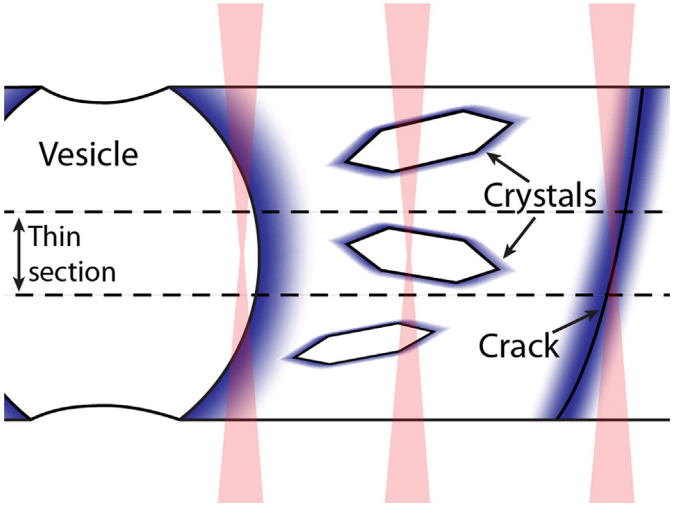

Fig. 4. Thickness issues when performing FTIR analyses on textured volcanic glass. The chances of artifacts due to the ray path of the light, geometrical effects and/or hidden objects are higher when measuring through a thick section rather than a thin section.

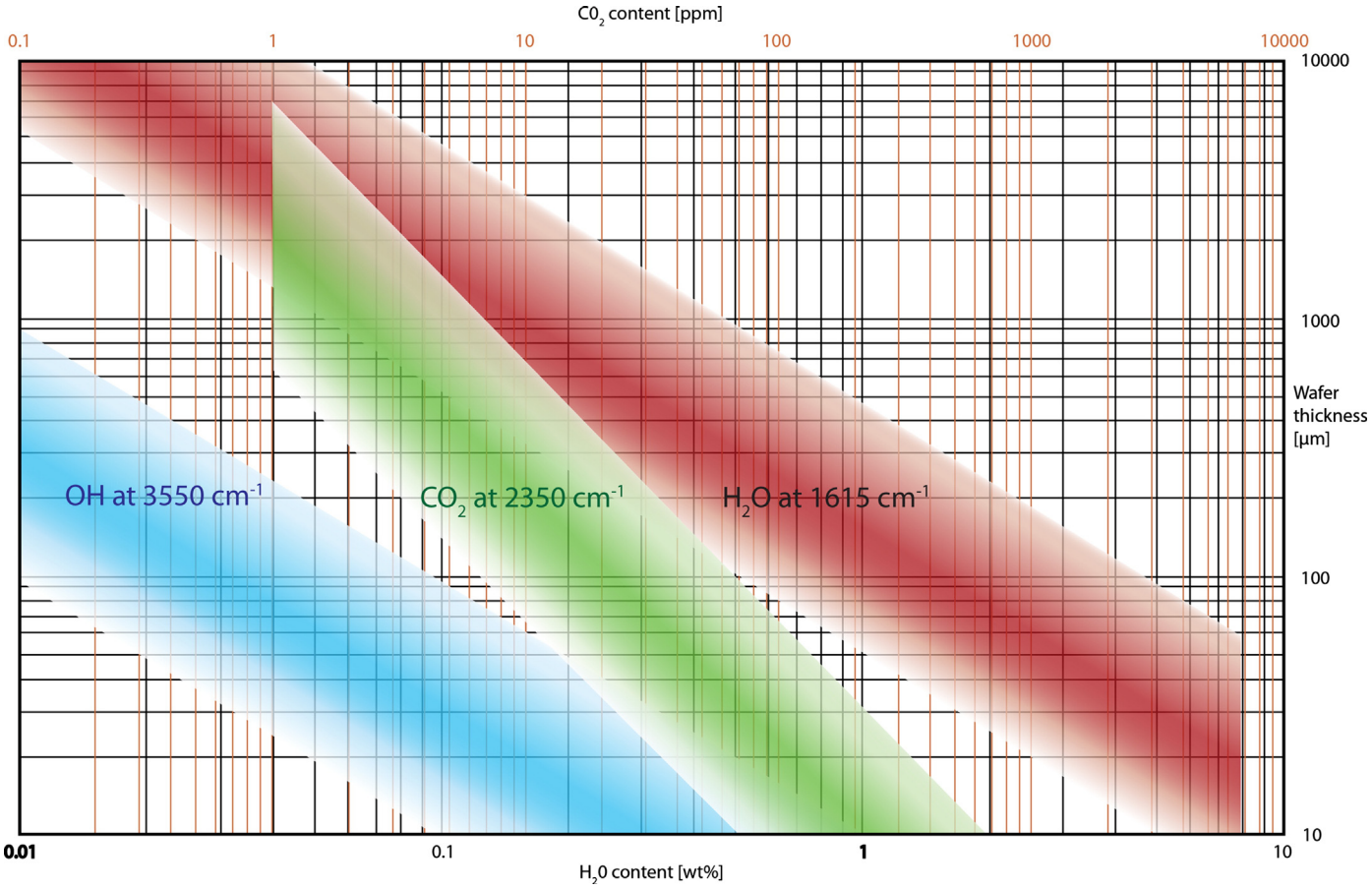

Fig. 5. Thickness estimations to consider before sample preparation. This is a rough estimate of ideal absorptivities for rhyolitic samples at different volatile concentrations and thicknesses. Blue: water in mid-IR, green: CO_2 in mid-IR, red: water in near-IR. The limits can be varied, depending on experimental setup. However, at the values between 0.2 and 0.7, signal-to-noise ratios are the highest (Schrader, 1995). Absorptivities for more mafic materials are slightly different, however, opacity of the sample may be an issue when measuring samples of high iron contents. Therefore, these numbers should only be considered as a rough guideline.

4.2. Thickness of the sample

To estimate the ideal thickness for a sample, its volatile content has to first be predicted and an absorbance be calculated from that prediction. Best results are achieved for absorbances between 0.2 and 0.7 (Schrader, 1995), but also at much higher absorbances, the detector may receive enough light depending on the sample and instrumental setup. If not enough light is transmitted to the detector (i.e., absorbances are too high), the detector may respond non-linearly and the height of the absorbance peak will no longer be proportional to species concentration and sample thickness. Fig. 5 shows estimated absorbances for the most common cases of rhyolitic glasses and can be used as a quick reference to calculate the necessary wafer thickness. These thicknesses should only be seen as approximate values and different values might be more appropriate for different reasons:

- If the sample shows opacity (e.g. mafic compositions), the sample has to be thinner to achieve a sufficiently strong signal. Absorption coefficients for rhyolitic compositions in Fig. 5 only differ slightly from basaltic absorption. Table 1 can be used as a rough guide for basalts as long as the sample is not too dark.
- If the sample contains crystals, cracks or vesicles, the sample may have to be thin to avoid hidden features within the thickness of the wafer. See Fig. 4.
- Geometrical effects throughout the sample can distort concentration patterns if the section is not cut parallel to the direction of the volatile gradient. This can be minimized by preparing thinner wafers and choosing locations where the distribution can be assumed to be homogeneous throughout the thickness of the sample, and perpendicular to the texture of interest (see Fig. 4).

Conversely, thin samples are problematic in three ways:

- Thin samples are difficult to handle and prepare. They can easily break or be lost.
- The accuracy of quantitative measurements of thin samples largely depends on the accuracy of thickness measurements. A nominally small error in thickness measurements can lead to large relative errors in composition quantification. If a sample measures 15 µm in thickness, and the thickness evaluation gives an error of ±2 µm, the overall error is larger than 25%, however, at a thickness of 150 µm the error is lowered by an order of magnitude.
- Large interference fringes in transmission spectra are very common in thin wafers, obstructing spectral information.

Properties of each individual sample have to be considered when targeting thicknesses during preparation. Heterogeneous samples and samples with unknown water contents should be polished to thinner wafers to keep the spatial resolution high and to avoid oversaturation of the detector.

4.3. Mounting and choice of adhesives

Samples that need to be doubly polished should be mounted on a slide. For structurally stable samples the first side can be polished without support. If the sample is fragile, vesicular or fractured, it will have to be impregnated with a bonding agent before the first polishing. Small

samples, such as crystals containing glass inclusions, also have to first be mounted to a slide using a resin or glue. Several different adhesives are commonly used and each has specific properties that have to be considered before use.

- Crystalbond™ 509 is an adhesive that can be melted onto the sample at ≈100 °C and removed with acetone. Crystalbond™ is a good choice for both adhesive and impregnation purposes as long as the samples are small. Handling is particularly easy and the mounted sample can be adjusted at any time. When one side of the sample is polished, the slide is heated to soften the crystal bond, and the sample can be flipped to the other side. Further advantages are its fast setting times and excellent solubility in acetone. Polishing should be done manually or at very slow speeds on a lap wheel to avoid softening of the Crystalbond™ due to heat production during preparation. For small samples and very porous samples that need large volumes to be filled, Crystalbond™ is preferred for its ease of handling, but it must be ensured that the short periods of heating during polishing do not alter the sample.
- Superglue (ethyl-2-cyanoacrylate) has a very defined chemical composition, is a strong adhesive and binds quickly at room temperature. It can be removed with acetone and residues can be easily spotted as a white film or fibrous material under the microscope. Superglue is stronger than Crystalbond™ if used in small volumes, which may prevent low surface area samples from flaking from the slide during polishing. Removing the glue takes longer compared to Crystalbond™, and the short hardening time can make handling challenging. Thinning the superglue with acetone is a good way of extending the working time, although it can produce bubbles in the set glue, which lowers the stability of the sample during cutting and polishing.
- Epoxy resins such as Araldite® or Epo-thin™ offer the highest stability of the adhesives and also act to fill sample voids. They are less brittle and so easier to handle as well, because they take longer to set, but are more difficult to be removed from the sample and the resultant sample spectra can thus show contamination. Care must be taken to ensure that the epoxy does not interfere with the measurements. Characteristic epoxy peaks are easy to detect and contaminated areas can be excluded from the sample data (Fig. 6).
- Orthodontic resin (Orthocryl®, Dentaurum) makes it easier to hold on to small samples while polishing the first side of the section and decreases the chances of loss during sample preparation. The Orthocryl consists of a powder and a liquid which together will take about 30 min to set. By alternating powder and liquid, a small mount of the Orthocryl can be built around the sample, giving it more bulk and stability for the polishing process. Any hydrophobic cream can be used (such as petroleum jelly) to keep the sample from sticking until the resin has fully set.

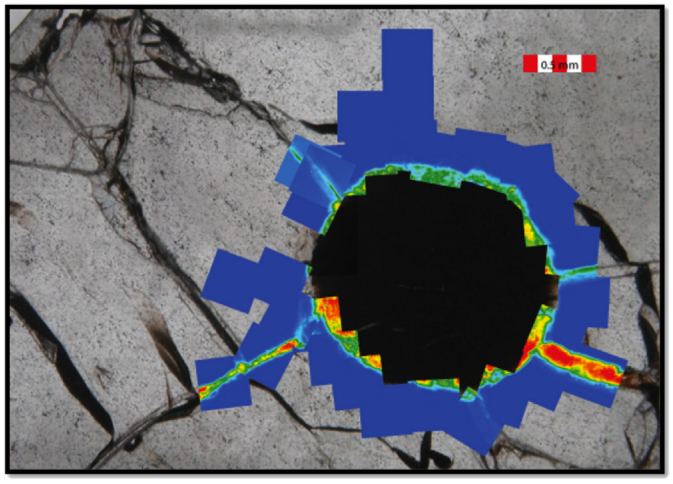

Fig. 6. Distribution of epoxy resin in a cracked glass around a spherulite (von Aulock et al., 2013) measured at 2973 cm^{-1}. False color map recorded with an FPA detector. Warm colors show elevated absorbances. The confined distribution helps to identify cracks and to dismiss data that could be affected by the presence of the resin.

4.4. Polishing

Samples have to be polished to ultrasmooth surfaces. For this, it is best to polish with decreasing grit sizes down to at least 1 μm; however, the best results are achieved with a grit size of 0.25 μm. The actual choice of material and grits depends on individual preferences and on properties of the samples, but a reliable choice is (in ISO/FEPA grit) P800–P1200–P1500–P2000 as wet silicon carbide papers. At P2000 the average particle diameter is 10.3 μm. Lower grain sizes are best polished under rolling grain. If the measured area contains cracks, bubbles, crystals or the sample is very small (≤3 mm, depending on the skills and equipment of the operator), care has to be taken not to polish shoulders into grain boundaries. Small samples should also be entirely covered with Crystalbond™ or other structuring adhesives if possible to make sure that the sides also remain embedded and enough surface area exists to effectively parallel polish the samples. However, it is possible to begin the grinding if the crystal protrudes from the crystal bond initially as long as the melt inclusion of interest is not too close to the protruding side. Embedding polishing aids of similar hardness, such as little pieces of colored glass, quartz or garnets at a distance from the sample, can help keep a parallel polish by adding resistance to the otherwise comparatively soft adhesive. If the samples have similar refractive indices as the adhesive, coloring of the sample with an acetone-soluble pen can make it easier to check the progress of the work. These can be avoided by using ceramic polishing dishes instead of felt polishing covers where possible, and minimizing overall polishing times. If the sample is very brittle or contains crystals or other objects that could break loose, felt is a better choice to avoid scratches. In any case, ample sample lubrication should be provided at all times. As lubricants, water can be used and for finer grit polishing, lubricants containing propylene glycol (available as common antifreeze for combustion engines) or similar are suitable choices.

4.5. Melt inclusions

Sample preparation for crystals with melt inclusions is similar to that for larger samples. Single crystals are mounted onto a glass slide using a removable adhesive. Prior to that, melt inclusions can be identified using immersion oil (with a refractive index identical to the mineral host). Because of the potential for boundary layer effects during trapping of melt inclusions, large melt inclusions (>50 μm) may be a better representation of the bulk volatile composition (Baker, 2008; Lu et al., 1995; Roedder, 1984). As crystals can break or become dislodged from the slide, polishing should be done gently either manually or using a lap at a low speed. Once one side of the crystal is polished until the desired melt inclusion is intersected, the crystal may be flipped onto its other side, either by dissolving the adhesive with acetone or by softening it on a hot plate. If the heating method is used, as soon as the crystal is flipped it should be pushed and moved gently to ensure that the flat side sits firmly on the glass slide to avoid making a wafer with a wedged shape.

5. New analytical capabilities

One of the most significant advances in for the FTIR analysis of volcanic glasses are the possibilities of 2-dimensional distribution measurements at spatial resolutions near- or at the diffraction limit at very high signal-to-noise ratios. Two of these techniques are discussed below, using either synchrotron light sources and/or focal plane array (FPA) detectors, combined with high precision motorized microscope stages (Della Ventura et al., 2010, 2014; Mormone et al., 2011).

5.1. Synchrotron IR sources

Synchrotron radiation is becoming more widely available to the scientific community and its use in FTIR microscopy opens up new possibilities for the microanalysis of volcanic glass. Synchrotron source FTIR offers many advantages over traditional laboratory-based instrumentation. These include spatial resolutions approaching the diffraction limit in the mid-IR region (Carr and Williams, 1997), and a significantly brighter light source, greatly improving the signal-to-noise of a system. The high collimation of a synchrotron source means more light passes through the aperture at small openings compared to globar sources. Miller and Smith (2005) show that at an opening of 10 μm, more than 80% of the radiation of a globar source is blocked by the aperture, compared to less than 20% of a synchrotron light source, and thus the signal-to-noise ratio remains high while fewer scans are required. These benefits collectively mean a user can analyze more samples in a given analytical session while still obtaining data of high quality, allowing highly detailed two dimensional chemical maps to be collected. Issues arise when mapping large areas however, due to the necessary but time consuming point-by-point raster mapping technique required to create these highly spatially resolved chemical images.

5.2. Focal plane array detectors and data volumes in imaging FTIR

FPA detectors, when combined with FTIR microscopy, allow for the fast micromapping of samples using a globar light source. Globar sources are ideal for these systems as FPA detectors require a source capable of illuminating all elements on the array simultaneously. Each individual detector element is capable of measuring the intensity of the light transmitted through a sample across the full spectral range of the system. The application of FPA detectors to FTIR microscopes has opened up many opportunities to map large areas in two dimensions at a fraction of the time it takes to map using a standard system, however typically these maps collect at lower spatial resolutions than achieved by point-by-point mapping at a synchrotron source. An innovative modification of the IRENI (IR Environmental Imaging) beamline, at the Synchrotron Radiation Centre (SRC), Wisconsin, USA, acts to solve this problem by splitting an incident synchrotron IR beam into 12 individual beams that are then used to illuminate an FPA detector (Nasse et al., 2011). There is very little reduction in synchrotron signal and this approach permits very rapid acquisition of 2D maps at the diffraction limit across the mid-IR region.

A recent and exciting application of the multi-beam FPA approach is three-dimensional spectral imaging with spectromicrotomography (Martin et al., 2013). Pioneered at the IRENI beamline, this approach operates like conventional X-ray CT microtomography insofar as the sample is rotated through the light path and several images are collected by the FPA at different sample positions. The effective wave attenuation that occurs during interaction with IR active species in the material is used to reconstruct individual images into a three-dimensional rendering of the object. Instead of material density, which the traditional X-ray CT approach tracks, it is the concentration and spatial distribution of IR-active chemicals within the sample that are portrayed in the reconstruction (Fig. 7). Fig. 7 shows one such 3D scan (Martin et al., 2013) and depicts the relative concentrations of silicate glass (brown) and hydroxyl groups (blue).

5.3. Data volumes and typical data collection parameters in imaging FTIR

A vast amount of data can be collected during FTIR measurements, particularly when using FPA microscopy. In most cases a resolution of between 4 cm^{-1} and 8 cm^{-1} is sufficient. The number of averaged scans per measurement point should be checked for new samples, but for most applications 64 or even 32 scans are adequate if the signal is at a reasonably high level to keep measurement times at a minimum without compromising the quality of the data. The choice of apodization function can lower the spectral resolution, however when focusing on relatively wide peaks across condensed phase samples, a high spectral resolution is not the highest priority. Therefore, a strong apodization function such as a three-term Blackman–Harris window is often used.

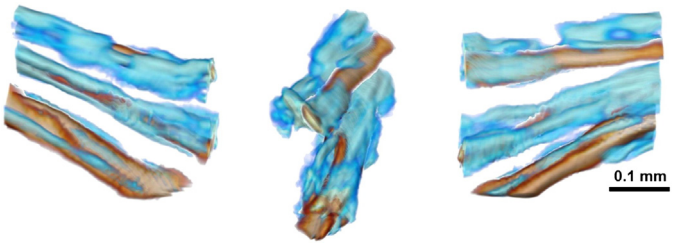

Fig. 7. Volcanic glass sample scanned at the IRENI beamline and rendered by 3D FTIR spectromicrotomography (Martin et al., 2013). A small volcanic glass filament from the recently erupted Puyehue–Cordon Caulle volcano in Chile was extracted from a volcanic bomb that was rapidly quenched at the time of eruption. This tiny filament of glass represents a frozen-in record of the formerly high-temperature melt and the magmatic water dissolved within this glass: specifically, molecular (H_2O) and hydroxyl groups (OH^-) bound to the silicate network are the target of analysis because these species control the physical properties of silicate melts, including its density and viscosity. Fifty spectral images over 180° were acquired and the 3D volume for every spectral point was reconstructed.

6. Data analysis for volatile concentration mapping in volcanic glass

Based on Beer's law, the volatile contents of a sample can be quantitatively determined using FTIR spectroscopy. This is the same for FTIR imaging analysis, except that it has to be decided whether constant physical parameters and curve parameters can be assumed for a range of different measurements. Slight peak shifts and different baseline levels throughout bulk spectra across a sample can introduce systematic errors. At the same time measurements should be kept as simple as possible to ensure that the results are reproducible. In most cases, the absorption is measured as the peak height, which does not mean that this method gives more reliable data. Especially at lower signal-to-noise ratios, the placement of a baseline can be difficult. However, most literature only presents extinction coefficients for peak height estimations. The baselines for the water-bands in the mid-IR range are commonly linear. Due to the sheer number of spectra collected in mapping and imaging spectroscopy, data have to be analyzed in bulk and not every individual spectrum can be checked. Therefore it is very important to check for systematic changes in the baseline. This can be caused by fringes at the base of an absorption peak or changes in the same spectral region (e.g. at 1830 cm^{-1}). Despite these limitations, a blanket treatment of all spectra of one map provides consistency, transparency and traceability of data analysis for peers.

6.1. Measurement of maps and ways to display results

In samples that are heavily textured and show complicated water distribution patterns, care has to be taken to choose the measurement distribution (e.g. spots, lines, dimensions or area to be analyzed). To ensure significance of the data, spot measurements or even a profile of the volatile distribution is often not sufficient and a 2-dimensional distribution map has to be measured. Hidden textures or chemical heterogeneities can often be identified by also measuring the area surrounding the area of interest (Fig. 4). This can either be done by using FPA detectors or by setting up a grid (map) measurement using a motorized microscope stage. However, contour maps displaying the distribution of the peak of interest are often misleading and may imply a higher lateral resolution across the map than actually measured. A grid where the measurement spots are highlighted is a simple way of showing the actual number of measurements taken across the grid while also showing enough of the photomicrograph of the sample behind (Fig. 8).

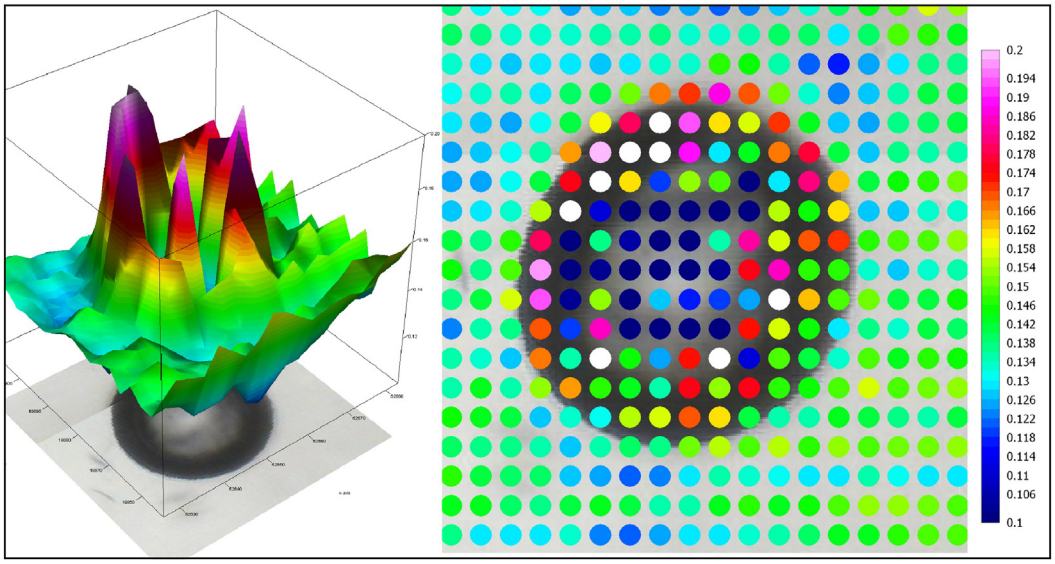

Fig. 8. Two ways of showing the same data of the integration of the total water band (at 3576 cm^{-1}) around a small bubble in volcanic glass. Showing spots instead of a 3D graphic reveals that the sharp increases are in fact just artifacts inside the bubble rather than increases of water around this particular bubble. Warm colors indicate high absorbtivities of total water. The bubble measures ≈30 μm in diameter.

7. Applications in volcanology

Recent publications have highlighted the importance of accurate and precise measurements of volatiles in volcanic glasses and melt inclusions at high spatial resolution using FTIR techniques. These include experimental studies (Iacovino et al., 2013; McIntosh et al., 2014) and studies on natural samples (e.g. Berlo et al., 2013; Cabrera et al., 2010; Castro and Dingwell, 2009; Liu et al., 2007; Owen et al., 2012; Watkins et al., 2012). High spatial resolutions make it possible to resolve the diffusional gradients that occur in silicate melts at temperatures and timescales common during volcanic eruptions (e.g. Cabrera et al., 2010; Castro and Dingwell, 2009; McIntosh et al., 2014; Watkins et al., 2012). Better constraints on volcanic temperatures and timescales are invaluable to improving and validating volcanic models. Recent work has highlighted that volatiles exsolve, re-dissolve and equilibrate in the melt during volcanic processes and volatile distribution profiles provide us with timescales of all three processes (von Aulock et al., 2013). Timescales of days to months were observed by von Aulock et al. (2013) in patterns of re-dissolution in perlitic, spherulitic obsidian by constraining the timescales at which volcanic glass alters in volcanic domes. Watkins et al. (2012) showed increased volatile contents towards vesicles in obsidian that indicate re-dissolution driven by pressure fluctuations at conduit levels in volcanoes, forming textures similar to the vesicle textures observed and described by Carey et al. (2012). In a study of water concentration gradients across small scale faults in obsidian, Cabrera et al. (2010) show that two juxtaposed layers of different water contents equilibrated within less than 30 min and adapted to lower pressures or higher temperatures. Von Aulock showed volatile equilibration in experimental samples at timescales greater than 12 h. The high spatial and quantitative resolutions now achievable using FTIR spectroscopy, particularly at a synchrotron source help to constrain volatile gradient profiles which can be used to distinguish processes modeled at different initial volatile contents, temperatures and pressures. Combining textural analysis with models of diffusion can give a better understanding of timescales of the growth and closure of vesicles and cracks (Carey et al., 2012; McIntosh et al., 2014; Watkins et al., 2012).

Melt inclusions in phenocrysts provide information on volatile contents of melts at the time of crystal growth (e.g. Metrich and Wallace, 2008; Wallace, 2005). Recent studies have defined volatile gradients in melt inclusions towards their crystal hosts and have used these to elucidate timescales of crystal ascent and/or re-equilibration related to the residence time in a magma chamber (e.g. Bucholz et al., 2013; Lloyd et al., 2012). Water in nominally anhydrous minerals can be measured down to small quantities of a few parts per million (Peslier, 2010). Effects of the orientation of the crystal lattice can be additionally controlled by using polarized light (e.g. Bellatreccia et al., 2005). Such studies can help to model water contents in a variety of geological environments such as the young moon (Hui et al., 2013) or the Earth's interior (Demouchy et al., 2006; Jacobsen et al., 2005). New techniques higher resolution and automated data collection make it now possible to measure more data points, with less signal to noise and reduced error bars. These data then give more insight into a greater range of magmatic regimes and properties while improving the quality of volatile content databases.

8. Conclusions

FTIR is a potent method for analyzing volatiles in volcanic glasses. New possibilities of increased spatial resolution and faster processing of arrays of data present the opportunity for both two and possibly three-dimensional chemical maps of volatile concentrations at diffraction-limited spatial resolutions in the mid-IR region. However, sample preparation and the choice of measurement parameters are still in the hands of the operator. In order to encourage the community of geosciences to use modern FTIR techniques such as FTIR microscopy coupled to an FPA detector, or synchrotron-sourced FTIR microscopy, we present an advice for the standardization of sample preparation, measurement and data analysis

Acknowledgments

We would like to thank Mark Tobin for his comments on early stages of this manuscript and his technical advice. This research was undertaken on the IRM beamline at the Australian Synchrotron, Victoria, Australia (FvA, BK and IS AS132/IRM/6707, FvA, BK and CO also rounds AS122/IRM/4990 and AS112/IRM/3893a + b). Funding for BK and FvA was provided by Marsden Fast Start (09-UO-017C), New Zealand.

HT acknowledges support from a Royal Society University Research Fellowship. Funding for JW was provided by National Science Foundation grant NSF-EAR 1249404. FvA acknowledges support from the European Research Council for the Starter Grant on Strain Localisation in Magmas (SLiM, nbr. 306488).

References

Agrinier, P., Jendrzejewski, N., 2000. Overcoming problems of density and thickness measurements in FTIR volatile determinations: a spectroscopic approach. Contributions to Mineralogy and Petrology 139, 265–272.

Applegarth, L.J., Tuffen, H., James, M.R., Pinkerton, H., Cashman, K.V., 2013. Direct observations of degassing-induced crystallization in basalts. Geology 41, 243–246.

Ardia, P., Di Muro, a., Giordano, D., Massare, D., Sanchez-Valle, C., Schmidt, M., 2014. Densification mechanisms of haplogranite glasses as a function of water content and pressure based on density and Raman data. Geochimica et Cosmochimica Acta 138, 158–180.

Baker, D.R., 2008. The fidelity of melt inclusions as records of melt composition. Contributions to Mineralogy and Petrology 156, 377–395.

Befus, K.S., Gardner, J.E., Zinke, R.W., 2012. Analyzing water contents in unexposed glass inclusions in quartz crystals. American Mineralogist 97, 1898–1904.

Behrens, H., Romano, C., Nowak, M., Holtz, F., Dingwell, D.B., 1996. Near-infrared spectroscopic determination of water species in glasses of the system MAlSi3O8 (M = Li, Na, K): an interlaboratory study. Chemical Geology 128, 41–63.

Behrens, H., Tamic, N., Holtz, F., 2004. Determination of the molar absorption coefficient for the infrared absorption band of CO_2 in rhyolitic glasses. American Mineralogist 5, 5–10.

Behrens, H., Roux, J., Neuville, D., Siemann, M., 2006. Quantification of dissolved H_2O in silicate glasses using confocal microRaman spectroscopy. Chemical Geology 229, 96–112.

Bellatreccia, F., Della Ventura, G., Ottolini, L., Libowitzky, E., Beran, A., 2005. The quantitative analysis of OH in vesuvianite: a polarized FTIR and SIMS study. Physics and Chemistry of Minerals 32, 65–76.

Berlo, K., Tuffen, H., Smith, V., Castro, J.M., Pyle, D., Mather, T., Geraki, K., 2013. Element variations in rhyolitic magma resulting from gas transport. Geochimica et Cosmochimica Acta 121, 436–451.

Bucholz, C.E., Gaetani, G.A., Behn, M.D., Shimizu, N., 2013. Post-entrapment modification of volatiles and oxygen fugacity in olivine-hosted melt inclusions. Earth and Planetary Science Letters 374, 145–155.

Bureau, H., Raepsaet, C., Khodja, H., Carraro, A., Aubaud, C., 2009. Determination of hydrogen content in geological samples using elastic recoil detection analysis (ERDA). Geochimica et Cosmochimica Acta 73, 3311–3322.

Cabrera, A., Weinberg, R.F., Wright, H.M.N., Zlotnik, S., Cas, R., 2010. Melt fracturing and healing: a mechanism for degassing and origin of silicic obsidian. Geology 39, 67–70.

Carey, R.J., Manga, M., Degruyter, W., Swanson, D., Houghton, B., Orr, T., Patrick, M., 2012. Externally triggered renewed bubble nucleation in basaltic magma: the 12 October 2008 eruption at Halemaumau Overlook vent, Klauea, Hawaii, USA. Journal of Geophysical Research 117, B11202.

Carr, G., Williams, G., 1997. Infrared microspectroscopy with synchrotron radiation. SPIE Conf. Proc. v3153, pp. 51–59.

Cashman, K.V., Sparks, R.S.J., 2013. How volcanoes work: a 25 year perspective. Geological Society of America Bulletin 125, 664–690.

Castro, J.M., Dingwell, D.B., 2009. Rapid ascent of rhyolitic magma at Chaitén volcano, Chile. Nature 461, 780–783.

Castro, J.M., Manga, M., Martin, M.C., 2005. Vesiculation rates of obsidian domes inferred from H_2O concentration profiles. Geophysical Research Letters 32, L21307.

Castro, J.M., Beck, P., Tuffen, H., Nichols, A.R.L., Dingwell, D.B., Martin, M.C., 2008. Timescales of spherulite crystallization in obsidian inferred from water concentration profiles. American Mineralogist 93, 1816–1822.

Castro, J.M., Cordonnier, B., Tuffen, H., Tobin, M.J., Puskar, L., Martin, M.C., Bechtel, H.A., 2012. The role of melt-fracture degassing in defusing explosive rhyolite eruptions at volcán Chaitén. Earth and Planetary Science Letters 333–334, 63–69.

Cherniak, D.J., Hervig, R.L., Koepke, J., Zhang, Y., Zhao, D., 2010. Analytical methods in diffusion studies. Reviews in Mineralogy and Geochemistry 72, 107–170.

Cocheo, P.A., 1994. The Solubility of Water in Basanitic Melts at Low Pressures(Ph.D. Thesis) Arizona State University.

Delaney, J., Karsten, J., 1981. Ion microprobe studies of water in silicate melts. Concentration-dependent water diffusion in obsidian. Earth and Planetary Science Letters 52, 191–202.

Della Ventura, G., Bellatreccia, F., Marcelli, A., Cestelli Guidi, M., Piccinini, M., Cavallo, A., Piochi, M., 2010. Application of micro-FTIR imaging in the Earth sciences. Analytical and Bioanalytical Chemistry 397, 2039–2049.

Della Ventura, G., Marcelli, A., Bellatreccia, F., 2014. SR-FTIR microscopy and FTIR imaging in the Earth sciences. Reviews in Mineralogy and Geochemistry 78, 447–479.

Demouchy, S., Jacobsen, S.D., Gaillard, F., Stern, C.R., 2006. Rapid magma ascent recorded by water diffusion profiles in mantle olivine. Geology 34, 429.

Denton, J., Tuffen, H., Gilbert, J., Odling, N., 2009. The hydration and alteration of perlite and rhyolite. Journal of the Geological Society 166, 895–904.

Devine, J., Gardner, J., Brack, H., Layne, G.D., Rutherford, M.J., 1995. Comparison of microanalytical methods for estimating H_2O contents of silicic volcanic glasses. American Mineralogist 80, 319–328.

Di Matteo, V., Carroll, M., Behrens, H., Vetere, F., Brooker, R., 2004. Water solubility in trachytic melts. Chemical Geology 213, 187–196.

Di Muro, A., Villemant, B., Montagnac, G., Scaillet, B., Reynard, B., 2006. Quantification of water content and speciation in natural silicic glasses (phonolite, dacite, rhyolite) by confocal microRaman spectrometry. Geochimica et Cosmochimica Acta 70, 2868–2884.

Dixon, J.E., Stolper, E., Delaney, J.R., 1988. Infrared spectroscopic measurements of CO_2 and H_2O in Juan de Fuca Ridge basaltic glasses. Earth and Planetary Science Letters 90, 87–104.

Dixon, J., Stolper, E., Holloway, J., 1995. An experimental study of water and carbon dioxide solubilities in mid-ocean ridge basaltic liquids. Part I: calibration and solubility models. Journal of Petrology 36, 1607–1631.

Dobson, P.F., Epstein, S., Stolper, E.M., 1989. Hydrogen isotope fractionation between coexisting vapor and silicate glasses and melts at low pressure. Geochimica et Cosmochimica Acta 53, 2723–2730.

Fine, G., Stolper, E., 1985. The speciation of carbon dioxide in sodium aluminosilicate glasses. Contributions to Mineralogy and Petrology 91, 105–121.

Gardner, J.E., Befus, K.S., Watkins, J.M., Hesse, M., Miller, N., 2012. Compositional gradients surrounding spherulites in obsidian and their relationship to spherulite growth and lava cooling. Bulletin of Volcanology 74, 1865–1879.

Gonnermann, H.M., Manga, M., 2005. Nonequilibrium magma degassing: results from modeling of the ca. 1340 A.D. eruption of Mono Craters, California. Earth and Planetary Science Letters 238, 1–16.

Hammer, J.E., Cashman, K.V., Hoblitt, R.P., Newman, S., 1999. Degassing and microlite crystallization during pre-climactic events of the 1991 eruption of Mt. Pinatubo, Philippines. Bulletin of Volcanology 60, 355–380.

Hauri, E., Wang, J., Dixon, J., King, P.L., Mandeville, C.W., Newman, S., 2002. SIMS analysis of volatiles in silicate glasses: 1. Calibration, matrix effects and comparisons with FTIR. Chemical Geology 183, 99–114.

Hervig, R.L., Dunbar, N., Westrich, H.R., Kyle, P., 1989. Pre-eruptive water content of rhyolitic magmas as determined by ion microprobe analyses of melt inclusions in phenocrysts. Journal of Volcanology and Geothermal Research 36, 293–302.

Hervig, R.L., Mazdab, F.K., Moore, G., McMillan, P.F., 2003. Melt inclusions in volcanic systems — methods, applications and problems. Volume 5 of Developments in VolcanologyElsevier.

Hess, K.U., Dingwell, D.B., 1996. Viscosities of hydrous leucogranitic melts: a non-Arrhenian model. The American Mineralogist 81, 1297–1300.

Hui, H., Peslier, A.H., Zhang, Y., Neal, C.R., 2013. Water in lunar anorthosites and evidence for a wet early moon. Nature Geoscience 6, 177–180.

Humphreys, M.C.S., Menand, T., Blundy, J.D., Klimm, K., 2008. Magma ascent rates in explosive eruptions: constraints from H_2O diffusion in melt inclusions. Earth and Planetary Science Letters 270, 25–40.

Iacovino, K., Moore, G., Roggensack, K., Oppenheimer, C., Kyle, P., 2013. H_2OCO_2 solubility in mafic alkaline magma: applications to volatile sources and degassing behavior at Erebus volcano, Antarctica. Contributions to Mineralogy and Petrology 166, 845–860.

Ihinger, P.D., Hervig, R.L., McMillan, P.F., Zhang, Y., Stolper, E.M., 1994. Analytical methods for volatiles in glasses. Reviews in Mineralogy and Geochemistry 30, 67–121.

Jacobsen, S.D., Demouchy, S., Frost, D.J., Ballaran, T.B., Kung, J., 2005. A systematic study of OH in hydrous wadsleyite from polarized FTIR spectroscopy and single-crystal X-ray diffraction: oxygen sites for hydrogen storage in Earth's interior. American Mineralogist 90, 61–70.

Jendrzejewski, N., Javoy, M., Trull, T., 1996. Mesures quantitatives de carbone et d'eau dans les verres basaltiques naturels par Spectroscopie Infrarouge. Partie II: l'eau. Comptes rendus de l'Académie des Sciences. Série 2. Sciences de la Terre et des Planètes 322, 735–742.

Johnson, E.R., Kamenetsky, V.S., McPhie, J., Wallace, P.J., 2011. Degassing of the H_2O-rich rhyolites of the Okataina Volcanic Center, Taupo Volcanic Zone, New Zealand. Geology 39, 311–314.

Kennedy, B., Jellinek, A., Russell, J., Nichols, A., Vigouroux, N., 2010. Time-and temperature-dependent conduit wall porosity: a key control on degassing and explosivity at Tarawera volcano, New Zealand. Earth and Planetary Science Letters 299, 126–137.

Kilgour, G., Blundy, J., Cashman, K., Mader, H.M., 2013. Small volume andesite magmas and melt–mush interactions at Ruapehu, New Zealand: evidence from melt inclusions. Contributions to Mineralogy and Petrology 166, 371–392.

King, P.L., Larsen, J.F., 2013. A micro-reflectance IR spectroscopy method for analyzing volatile species in basaltic, andesitic, phonolitic, and rhyolitic glasses. American Mineralogist 98, 1162–1171.

King, P., Vennemann, T., Holloway, J.R., Hervig, R.L., Lowenstern, J.B., Forneris, J.F., 2002. Analytical techniques for volatiles: a case study using intermediate (andesitic) glasses. American Mineralogist 87, 1077–1089.

Lange, R., 1997. A revised model for the density and thermal expansivity of K_2O–Na_2O–CaO–MgO–Al_2O_3–SiO_2 liquids from 700 to 1900 K: extension to crustal magmatic temperatures. Contributions to Mineralogy and Petrology 1–11.

Lange, R.A., Carmichael, I.S., 1987. Densities of Na_2O–K_2O–MgO–MgO–FeO–Fe_2O_3–Al_3O_3–TiO_2–SiO_2 liquids: new measurements and derived partial molar properties. Geochimica et Cosmochimica Acta 51, 2931–2946.

Le Losq, C., Neuville, D.R., Moretti, R., Roux, J., 2012. Determination of water content in silicate glasses using Raman spectrometry: implications for the study of explosive volcanism. American Mineralogist 97, 779–790.

Leschik, M., Heide, G., Frischat, G.H., Behrens, H., Wiedenbeck, M., Wagner, N., Heide, K., Geissler, H., Reinholz, U., 2004. Determination of H_2O and D_2O contents in rhyolitic glasses. Physics and Chemistry of Glasses 45, 238–251.

Liritzis, I., Laskaris, N., 2011. Fifty years of obsidian hydration dating in archaeology. Journal of Non-Crystalline Solids 357, 2011–2023.

Liu, Y., Anderson, A.T., Wilson, C.J.N., 2007. Melt pockets in phenocrysts and decompression rates of silicic magmas before fragmentation. Journal of Geophysical Research 112, 12.

Lloyd, A.S., Plank, T., Ruprecht, P., Hauri, E.H., Rose, W., 2012. Volatile loss from melt inclusions in pyroclasts of differing sizes. Contributions to Mineralogy and Petrology 165, 129–153.

Lowenstern, J.B., 1995. Applications of silicate-melt inclusions to the study of magmatic volatiles. Magmas, fluids and ore deposits. Mineralogical Association of Canada Short Course 23, pp. 71–99.

Lowenstern, J.B., Pitcher, B.W., 2013. Analysis of H_2O in silicate glass using attenuated total reflectance (ATR) micro-FTIR spectroscopy. American Mineralogist 98, 1660–1668.

Lu, F., Anderson, A.T., Davis, A., 1995. Diffusional gradients at the crystal/melt interface and their effect on the compositions of melt inclusions. The Journal of Geology 103, 591–597.

Mandeville, C., Webster, J.D., Rutherford, M.J., Taylor, B.E., Timbal, A., Faure, K., 2002. Determination of molar absorptivities for infrared absorption bands of H_2O in andesitic glasses. American Mineralogist 87, 813–821.
Martin, M.C., Dabat-Blondeau, C., Unger, M., Sedlmair, J., Parkinson, D.Y., Bechtel, H.a, Illman, B., Castro, J.M., Keiluweit, M., Buschke, D., Ogle, B., Nasse, M.J., Hirschmugl, C.J., 2013. 3D spectral imaging with synchrotron Fourier transform infrared spectro-microtomography. Nature Methods 10, 861–864.
McIntosh, I., Llewellin, E., Humphreys, M., Nichols, A., Burgisser, A., Schipper, C., Larsen, J., 2014. Distribution of dissolved water in magmatic glass records growth and resorption of bubbles. Earth and Planetary Science Letters 401, 1–11.
Metrich, N., Wallace, P.J., 2008. Volatile abundances in basaltic magmas and their degassing paths tracked by melt inclusions. Reviews in Mineralogy and Geochemistry 69, 363–402.
Miller, L.M., Smith, R.J., 2005. Synchrotrons versus globars, point-detectors versus focal plane arrays: selecting the best source and detector for specific infrared microspectroscopy and imaging applications. Vibrational Spectroscopy 38, 237–240.
Miwa, T., Toramaru, A., 2013. Conduit process in vulcanian eruptions at Sakurajima volcano, Japan: inference from comparison of volcanic ash with pressure wave and seismic data. Bulletin of Volcanology 75, 685.
Mongrain, J., Larsen, J.F., King, P.L., 2008. Rapid water exsolution, degassing and bubble collapse observed experimentally in K-phonolite melts. Journal of Volcanology and Geothermal Research 173, 178–184.
Mormone, a, Piochi, M., Bellatreccia, F., De Astis, G., Moretti, R., Ventura, G.D., Cavallo, a, Mangiacapra, a, 2011. A CO_2-rich magma source beneath the Phlegraean Volcanic District (Southern Italy): evidence from a melt inclusion study. Chemical Geology 287, 66–80.
Nakamoto, K., 2006. Infrared and Raman Spectra of Inorganic and Coordination Compounds. John Wiley & Sons, Ltd.
Nasse, M.J., Mattson, E.C., Reininger, R., Kubala, T., Janowski, S., El-Bayyari, Z., Hirschmugl, C. J., 2011. Multi-beam synchrotron infrared chemical imaging with high spatial resolution: beamline realization and first reports on image restoration. Nuclear Instruments and Methods in Physics Research Section A: Accelerators, Spectrometers, Detectors and Associated Equipment 649, 172–176.
Newman, S., Stolper, E., Epstein, S., 1986. Measurement of water in rhyolitic glasses — calibration of an infrared spectroscopic technique. American Mineralogist 71, 11–12.
Newman, S., Epstein, S., Stolper, E.M., 1988. Water, carbon dioxide, and hydrogen isotopes in glasses from the ca. 1340 A.D. eruption of the Mono Craters, California: constraints on degassing phenomena and initial volatile content. Journal of Volcanology and Geothermal Research 35, 75–96.
Nichols, A.R.L., Wysoczanski, R.J., 2007. Using micro-FTIR spectroscopy to measure volatile contents in small and unexposed inclusions hosted in olivine crystals. Chemical Geology 242, 371–384.
Nichols, A., Potuzak, M., Dingwell, D., 2009. Cooling rates of basaltic hyaloclastites and pillow lava glasses from the HSDP2 drill core. Geochimica et Cosmochimica Acta 73, 1052–1066.
Ochs III, F.A., Lange, R.A., 1999. The density of hydrous magmatic liquids. Science 283, 1314–1317.
Okumura, S., 2005. Molar absorptivities of OH and H_2O in rhyolitic glass at room temperature and at 400–600 C. Am. Mineral. 90 (2–3), 441–447.
Okumura, S., Nakamura, M., Nakashima, S., 2003. Determination of molar absorptivity of IR fundamental OH-stretching vibration in rhyolitic glasses. American Mineralogist 88, 1657–1662.
Owen, J., Tuffen, H., McGarvie, D.W., 2012. Using dissolved H_2O in rhyolitic glasses to estimate palaeo-ice thickness during a subglacial eruption at Bláhnúkur (Torfajökull, Iceland). Bulletin of Volcanology 74, 1355–1378.
Peslier, A.H., 2010. A review of water contents of nominally anhydrous natural minerals in the mantles of Earth, Mars and the Moon. Journal of Volcanology and Geothermal Research 197, 239–258.
Plank, T., Kelley, K.A., Zimmer, M.M., Hauri, E.H., Wallace, P.J., 2013. Why do mafic arc magmas contain ~4 wt.% water on average? Earth and Planetary Science Letters 364, 168–179.
Richet, P., Whittington, A., Holtz, F., Behrens, H., Ohlhorst, S., Wilke, M., 2000. Water and the density of silicate glasses. Contributions to Mineralogy and Petrology 138, 337–347.
Roedder, E., 1984. Reviews in mineralogy. Fluid Inclusions, vol. 12. Mineralogical Society of America.
Rust, A., Manga, M., Cashman, K.V., 2003. Determining flow type, shear rate and shear stress in magmas from bubble shapes and orientations. Journal of Volcanology and Geothermal Research 122, 111–132.
Schipper, C.I., White, J.D.L., Nichols, A.R.L., Burgisser, A., Hellebrand, E., et al., 2012. Incipient melt segregation as preserved in subaqueous pyroclasts. Geology 40, 355–358.
Schrader, B., 1995. Infrared and Raman spectroscopy: methods and applications, 1 edition. VCH Verlagsgesellschaft mbH.
Seaman, S.J., 2013. Microtexture development during rapid cooling in three rhyolitic lava flows. American Mineralogist 98, 304–318.
Shaw, A., Hauri, E., Fischer, T., Hilton, D., Kelley, K., 2008. Hydrogen isotopes in Mariana arc melt inclusions: implications for subduction dehydration and the deep-Earth water cycle. Earth and Planetary Science Letters 275, 138–145.
Silver, L., Stolper, E., 1989. Water in albitic glasses. Journal of Petrology 30, 667–709.
Silver, L.A., Ihinger, P.D., Stolper, E.M., 1990. The influence of bulk composition on the speciation of water in silicate glasses. Contributions to Mineralogy and Petrology 104, 142–162.
Sparks, R.S.J., 1978. The dynamics of bubble formation and growth in magmas: a review and analysis. Journal of Volcanology and Geothermal Research 3, 1–37.
Spilliaert, N., Allard, P., Métrich, N., Sobolev, A.V., 2006. Melt inclusion record of the conditions of ascent, degassing, and extrusion of volatile-rich alkali basalt during the powerful 2002 flank eruption of Mount Etna (Italy). Journal of Geophysical Research 111, B04203.
Stevenson, C.M., Novak, S.W., 2011. Obsidian hydration dating by infrared spectroscopy: method and calibration. Journal of Archaeological Science 38, 1716–1726.
Stolper, E.M., 1982a. The speciation of water in silicate melts. Geochimica et Cosmochimica Acta 46, 2609–2620.
Stolper, E.M., 1982b. Water in silicate glasses: an infrared spectroscopic study. Contributions to Mineralogy and Petrology 81, 1–17.
Stolper, E., Fine, G., Johnson, W.L., Newman, S., 1987. Solubility of carbon dioxide in albitic melt. American Mineralogist 72, 1071–1085.
Thibault, Y., Holloway, J.R., 1994. Solubility of CO_2 in a Ca-rich leucitite: effects of pressure, temperature, and oxygen fugacity. Contributions to Mineralogy and Petrology 116, 216–224.
Tuffen, H., Owen, J., Applegarth, L., 2012. Measurement of volatile concentrations in volcanic glasses using thermogravimetric analysis: comparison with micro-analytical methods. EGU General Assembly 2012. 14, p. 11347.
Turek, A., Riddle, C., Cozens, B., Tetley, N., 1976. Determination of chemical water in rock analysis by Karl Fischer titration. Chemical Geology 17, 261–267.
Varela, M., Metrich, N., 2000. Carbon in olivines of chondritic meteorites. Geochimica et Cosmochimica Acta 64, 3433–3438.
Varela, M., Metrich, N., Bonnin-Mosbah, M., Kurat, G., 2000. Carbon in glass inclusions of Allende, Vigarano, Bali, and Kaba (CV3) olivines. Geochimica et Cosmochimica Acta 64, 3923–3930.
Ventura, G.D., Radica, F., Bellatreccia, F., Cavallo, A., Capitelli, F., Harley, S., 2012. Quantitative analysis of H_2O and CO_2 in cordierite using polarized FTIR spectroscopy. Contributions to Mineralogy and Petrology 164, 881–894.
von Aulock, F., Nichols, A., Kennedy, B., Oze, C., 2013. Timescales of texture development in a cooling lava dome. Geochimica et Cosmochimica Acta 114, 72–80.
Wallace, P.J., 2005. Volatiles in subduction zone magmas: concentrations and fluxes based on melt inclusion and volcanic gas data. Journal of Volcanology and Geothermal Research 140, 217–240.
Wallace, P., Anderson, A.T., Davis, A.M., 1999. Gradients in H_2O, CO_2, and exsolved gas in a large-volume silicic magma system: Interpreting the record preserved in melt inclusions from the Bishop Tuff. J. Geophys. Res. 104 (B9), 20097–20122.
Watkins, J.M., Manga, M., Huber, C., Martin, M., 2008. Diffusion-controlled spherulite growth in obsidian inferred from H_2O concentration profiles. Contributions to Mineralogy and Petrology 157, 163–172.
Watkins, J.M., Manga, M., DePaolo, D.J., 2012. Bubble geobarometry: A record of pressure changes, degassing, and regassing at Mono Craters. California, Geology 40 (8), 699–702.
Weaver, S.L., Wallace, P.J., Johnston, A.D., 2011. A comparative study of continental vs. intraoceanic arc mantle melting: experimentally determined phase relations of hydrous primitive melts. Earth and Planetary Science Letters 308, 97–106.
Weaver, S.L., Wallace, P.J., Johnston, D.A., 2013. Experimental constraints on the origins of primitive potassic lavas from the Trans-Mexican Volcanic Belt. Contributions to Mineralogy and Petrology 166, 825–843.
Weber, R.M., Wallace, P.J., Johnston, D.A., 2011. Experimental insights into the formation of high-Mg basaltic andesites in the trans-Mexican volcanic belt. Contrib. to Mineral. Petrol. 163 (5), 825–840.
Westrich, H.R., 1987. Determination of water in volcanic glasses by Karl Fischer titration. Chemical Geology 63, 335–340.
Wright, H.M., Cashman, K., Rosi, M., Cioni, R., 2007. Breadcrust bombs as indicators of vulcanian eruption dynamics at Guagua Pichincha volcano, Ecuador. Bulletin of Volcanology 69, 281–300.
Wysoczanski, R.J., Tani, K., 2006. Spectroscopic FTIR imaging of water species in silicic volcanic glasses and melt inclusions: an example from the Izu–Bonin arc. Journal of Volcanology and Geothermal Research 156, 302–314.
Yamashita, S., Kitamura, T., Kusakabe, M., 1997. Infrared spectroscopy of hydrous glasses of arc magma compositions. Geochemical Journal 31, 169–174.
Zhang, Y., 1999. H_2O in rhyolitic glasses and melts: measurement, speciation, solubility, and diffusion. Reviews of Geophysics and Space Physics 37, 493–516.
Zhang, Y., Belcher, R., Ihinger, P.D., Wang, L., Xu, Z., Newman, S., 1997. New calibration of infrared measurement of dissolved water in rhyolitic glasses. Geochimica et Cosmochimica Acta 61, 3089–3100.
Zhang, Y., Xu, Z., Behrens, H., 2000. Hydrous species geospeedometer in rhyolite: improved calibration and application. Geochimica et Cosmochimica Acta 64, 3347–3355.
Zhang, M., Salje, E., Bismayer, U., Groat, L.A., Malcherek, T., 2002. Metamictization and recrystallization of titanite: an infrared spectroscopic study. American Mineralogist 87, 882–890.